A Context-Aware Cognitive SIMO Transceiver for Increased LTE-HetNet System-Level DL-Throughput

(*Invited Paper*)

Imen Mrissa, Faouzi Bellili, Sofiène Affes, and Alex Stéphenne
INRS-EMT, 800 De La Gauchetiere Ouest, Suite 6900, Montreal (Quebec), H5A 1K6, Canada.
Emails: {mrissa, bellili, affes, stephenne}@emt.inrs.ca

***Abstract*—In this paper, we design a new single-input multiple-output (SIMO) context-aware cognitive transceiver (CTR) that is able to switch to the best performing modem in terms of link-level throughput. On the top of conventional adaptive modulation and coding (AMC), we allow the context-aware CTR to make best selection among three different pilot-utilization modes: conventional decision-aided (DA) or pilot-assisted, non-DA (NDA) or blind, and NDA with pilot which is a newly proposed hybrid version between the DA and NDA modes. We also enable the CTR to make best selection between two different channel identification schemes: conventional least-square (LS) and newly developed maximum-likelihood (ML) estimators. Depending on whether pilot symbols can be properly exploited or not at the receiver, we further enable the CTR to make best selection among two data detection modes: coherent or differential. Owing to extensive and exhaustive simulations on the downlink (DL) of a long-term evolution (LTE) heterogeneous network (HetNet), we are able draw out the decision rules of the new CTR that identify the best combination triplet of pilot-use, channel-identification, and data-detection modes to achieve the best link-level throughput at any operating condition in terms of channel type, mobile speed, signal-to-noise ratio (SNR), and channel quality indicator (CQI). Realistic extensive simulations at the system level suggest that the new context-aware CTR outperforms the conventional transceiver (i.e., pilot-assisted LS-type channel estimation with coherent detection) by as much as 40 and 45% gains in average and cell-edge (i.e., 5-percentile) total throughput per macro-area with 10 pico-cells each, respectively.**

I. Introduction

One of the strongest driving forces for wireless technology evolution today is 4G (4th Generation), also known as LTE-Advanced (Long Term Evolution) or IMT-Advanced (International Mobile Telecommunications) [1], which promises to encompass two main legacy technologies among others, namely cellular and WLAN (id., IEEE 802.xx). 4G promises to deliver high-speed wireless data transmission services at much lower costs and latency while providing much higher rates, spectrum efficiency and coverage. Most importantly, it promises the provision of future high-speed wireless data services everywhere closer to the mobile user in a seamless and versatile fashion, no matter what the surrounding environment and link conditions are. This stringent requirement calls for the development of new cognitive transceivers that are capable of promptly and properly self-adapting to variable operating conditions in order to constantly maximize their performance.

It is precisely in this vibrant research context that we get onto the emerging cognitive radio [2], [3] from a rather uncommon perspective today. Indeed, cognitive radio is reduced in most recent works to one of its two primary objectives: exploit efficiently the radio spectrum with dynamic spectrum access (DSA) that allocates the least occupied frequencies, though licensed and reserved, to secondary users who are short of bandwidth [4]- [6]. Here we take up its second primary objective of providing highly reliable communications anywhere anytime, so far addressed in a conventional manner, but rarely tackled today from a new level of "cognitive wireless communications" [3] where cognition could possibly handle many dynamic reconfiguration dimensions other than spectrum allocation, the conventional one. In this contribution, we aim at developing a new context-aware CTR which is able to self-adjust its antenna-array processing structure and air-interface configuration for optimum performance. Explicitly, we developed a new context-aware CTR that is able to select the best combination triplet of pilot-use, channel-identification, and data-detection modes that achieve the best link-level throughput against channel conditions in terms of channel type, mobile speed, SNR, and CQI. Realistic extensive simulations at the system level suggest that the new context-aware CTR outperforms the conventional transceiver (i.e., pilot-assisted LS-type channel estimation with coherent detection) by as much as 40 and 45% gains in average and cell-edge (i.e., 5-percentile) total throughput per macro-area with 10 pico-cells each, respectively.

The remainder of this paper is structured as follows. In Section II, we introduce the context-aware CTR modes along with the different channel estimation schemes. In Section III, exhaustive computer simulations are presented and discussed in order to assess and illustrate the tremendous performance gains of the proposed CTR. Finally, concluding remarks are drawn out in Section IV.

II. Context-aware cognitive transceiver modes

A. DA or pilot-assisted mode

Pilot symbols are reference (i.e., known) symbols inserted according to a predefined mapping to be used by the receiver for channel estimation and synchronization purposes. The LTE DL pilot mapping is described in Fig. 1.

1) LS channel estimator: This conventional estimator uses pilot symbols to estimate the channel by minimizing the squared difference between the received signal and the known pilot symbols. Let $y_{i,\mathrm{DA}}$ denote the received signal on pilot sub-carrier i among N_{pilot} pilot sub-carriers at the OFDM pilot symbol index t. For convenience, we will henceforth omit the time index t. The transmitted pilot symbol $x_{i,\mathrm{DA}}$ is related to $y_{i,\mathrm{DA}}$ as follows:

$$y_{i,\mathrm{DA}} = h_i x_{i,\mathrm{DA}} + n_i \qquad i = 0, 1, ..., N_{pilot} - 1 \tag{1}$$

where h_i is the complex channel coefficient and n_i is a zero-mean Gaussian noise. The matrix notation of (1) is given by:

$$\mathbf{y}_{\mathrm{DA}} = \mathbf{X}_{\mathrm{DA}}\mathbf{h} + \mathbf{n} \tag{2}$$

where $\mathbf{X}_{\mathrm{DA}} = \mathrm{diag}\left\{x_{0,\mathrm{DA}}, x_{1,\mathrm{DA}}, \ldots, x_{N_{pilot}-1,\mathrm{DA}}\right\}$, $\mathbf{h} = [h_0, h_1, ..., h_{N_{pilot}-1}]^T$, and $\mathbf{n} = [n_0, n_1, ..., n_{N_{pilot}-1}]^T$ is the i.i.d complex zero-mean Gaussian noise vector. The LS algorithm aims at minimizing $(\mathbf{y}_{DA} - \mathbf{X}_{DA}\mathbf{h})^{\dagger}(\mathbf{y}_{\mathrm{DA}} - \mathbf{X}_{\mathrm{DA}}\mathbf{h})$ ($\dagger$ denotes matrix Hermitian transpose) to estimate the channel frequency response thereby leading to [7]:

$$\widehat{\mathbf{h}}_{\mathrm{LS}} = \mathbf{X}_{\mathrm{DA}}^{-1}\mathbf{y}_{\mathrm{DA}}, \tag{3}$$

Work supported by the CREATE PERSWADE <www.create-perswade.ca> and the Discovery Grants Programs of NSERC and a Discovery Accelerator Supplement (DAS) Award from NSERC.

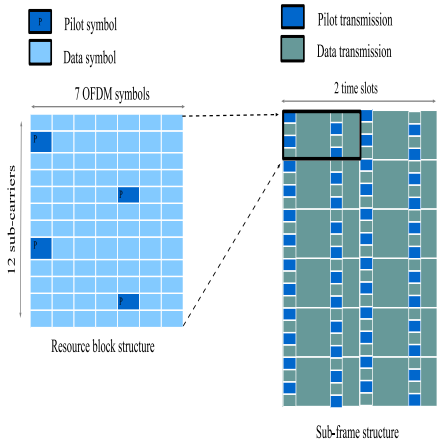

Fig. 1. LTE downlink pilot mapping.

where $\mathbf{A}^{-1}$ denotes the matrix inverse. The estimates for the channel coefficients at non-pilot subcarriers can then be easily obtained by interpolation [10]. However, when the channel is fast fading (i.e., high user velocity), the pilot symbols spacing may not be sufficient to enable proper tracking of the channel variations. Moreover, increasing pilot overhead leads to a throughput decrease which is not desirable for any communication system.

2) ML estimator: Here, we consider the ML channel estimator developed in [8]. For each OFDM symbol, the DA ML estimator captures the channel's time variations via a polynomial-in-time expansion of order $(J-1)$. In fact, the channel over each $\{r^{th}\}_{r=1}^{N_r}$ antenna branch and the i^{th} subcarrier, in a SIMO system, is modeled as follows [9]:

$$h_{i,r}(t_n) = \sum_{j=0}^{J-1} c_{i,r}^{(j)} t_n^j + REM_J^{(i,r)}(t_n). \tag{4}$$

Here, $t_n = nT_s$ with T_s being the sampling period. The polynomial order $J-1$ is a Doppler-dependent parameter optimized in [8]. Moreover, $c_{i,r}^{(j)}$ is the j^{th} coefficient of the channel polynomial approximation over the i^{th} sub-carrier and the r^{th} branch. As will be explained shortly, the term $REM_J^{(i,r)}(t_n)$ refers to the remainder of the Taylor series expansion which can be driven to zero by choosing an approximation window of sufficiently small size thereby yielding the following accurate approximation [8]:

$$h_{i,r}(t_n) = \sum_{j=0}^{J-1} c_{i,r}^{(j)} t_n^j. \tag{5}$$

Channel estimation is performed independently over each pilot sub-carrier. For the sake of simplicity, we also omit the sub-carrier index in the remainder of this paper.
To use a small model order $J-1$ in (4) and thereby avoid costly inversions of large-size matrices, the new DA ML estimator partitions the whole observation window into K local approximation windows of the same size. Then, it maximizes the probability density function (pdf) of the locally-observed vectors, $\mathbf{y}_{\text{DA}}^{(k)}$, parametrized by $\mathbf{c}_k$:

$$p(\mathbf{y}_{\text{DA}}^{(k)};\mathbf{c}_k|\mathbf{B}_k) = \frac{1}{(2\pi\sigma^2)^{N_{\text{DA}}N_r}} \exp\left\{-\frac{1}{2\sigma^2}\left[\mathbf{y}_{\text{DA}}^{(k)}-\mathbf{B}_k\mathbf{c}_k\right]^H\left[\mathbf{y}_{\text{DA}}^{(k)}-\mathbf{B}_k\mathbf{c}_k\right]\right\}, \tag{6}$$

where $\mathbf{c}_k$ is a vector containing the unknown approximation polynomial coefficients over the k^{th} approximation window (i.e., for all the antenna branches) defined as $\mathbf{c}_k = [\mathbf{c}_{k,1}^T, \mathbf{c}_{k,2}^T, ..., \mathbf{c}_{k,N_r}^T]^T$ with $\mathbf{c}_{k,r} = [c_{k,r}^{(0)}, c_{k,r}^{(1)}, ..., c_{k,r}^{(J-1)}]^T$ where $c_{k,r}^{(j)}$ is the j^{th} coefficient of the channel polynomial approximation over the i^{th} sub-carrier, the k^{th} approximation window and the r^{th} branch and σ^2 defines the noise variance. In (6), $\mathbf{y}_{\text{DA}}^{(k)} = [\mathbf{y}_{1,\text{DA}}^{(k)}\, \mathbf{y}_{2,\text{DA}}^{(k)} \cdots \mathbf{y}_{N_r,\text{DA}}^{(k)}]^T$ with $\mathbf{y}_{r,\text{DA}}^{(k)}$ being the received pilot samples over the antenna element r within the k^{th} approximation window, i.e., $\mathbf{y}_{r,\text{DA}}^{(k)} = [y_r^{(k)}(t_1)\, y_r^{(k)}(t_2) \ldots y_r^{(k)}(t_{P_{\text{DA}}})]$. Here P_{DA} is the number of pilot symbols in each approximation window which is covering N_{DA} pilot and non-pilot received samples. The approximation window size N_{DA} is another Doppler-dependent design parameter optimized in [8]. Moreover $\mathbf{B}_k$ is a $P_{\text{DA}}N_r \times JN_r$ block-diagonal matrix defined as $\mathbf{B}_k = \text{blkdiag}\{\mathbf{A}_k\mathbf{T}, \mathbf{A}_k\mathbf{T}, ..., \mathbf{A}_k\mathbf{T}\}$. Here, $\mathbf{A}_k$ is the $P_{\text{DA}} \times P_{\text{DA}}$ diagonal matrix of the transmitted pilot symbols within the k^{th} observation window, i.e., $\mathbf{A}_k = \text{diag}\{a_k(t_1), a_k(t_2), ..., a_k(t_{P_{\text{DA}}})\}$, and $\mathbf{T}$ is a Vandermonde matrix given by:

$$\mathbf{T} = \begin{pmatrix} 1 & t_1 & \ldots & t_1^{J-1} \\ 1 & t_2 & \ldots & t_2^{J-1} \\ \vdots & \vdots & \ddots & \vdots \\ 1 & t_{P_{DA}} & \ldots & t_{P_{DA}}^{J-1} \end{pmatrix}. \tag{7}$$

The estimate of the channel coefficients over all the receiving antenna branches are obtained by setting the partial derivative of (6) [or its natural logarithm] to zero yielding:

$$\widehat{\mathbf{c}}_{k,\text{DA}} = \left(\mathbf{B}_k^\dagger \mathbf{B}_k\right)^{-1}\mathbf{B}_k^\dagger \mathbf{y}_{\text{DA}}^{(k)}, \tag{8}$$

from which the DA ML estimates for the channel coefficients at both pilot and non-pilot positions are obtained by injecting the estimates of the polynomial coefficients established in (8) back into (4).

B. NDA with pilot or hybrid mode

Ensuring reliable communications is the purpose of all wireless communication systems. However, receiver mobility and surrounding scatterers' motion make channel estimation accuracy a truly challenging task. For that reason, pilot symbols that are inserted far apart, in the time-frequency grid, do not enable accurate tracking of fast-varying channels. Information carried in data symbols is hereafter exploited in a hybrid channel identification scheme in order to enhance the system performance.

1) NDA w. pilot RLS estimator: At OFDM symbol $t+1$, we use preceding transmitted signals as a training sequence of t symbols. In fact, the channel estimate, $\widehat{\mathbf{H}}_{t+1}$, at OFDM symbol $t+1$ is obtained using the weighted LS method as follows [11]:

$$\widehat{\mathbf{H}}_{t+1} = \underset{\widehat{\mathbf{H}}}{\text{argmin}} \sum_{w=1}^{t} \beta_w \|\mathbf{y}_w - \widehat{\mathbf{H}}\mathbf{Q}_w x_w\|^2, \tag{9}$$

where the channel variation $\mathcal{H}$ is approximated to the D^{th} order Taylor series expansion according to the OFDM symbol instance m, i.e.: $\mathcal{H}_w \simeq \sum_{d=0}^{D} w^d \mathcal{H}^{<d>} = \mathbf{H}\mathbf{Q}_w$ with $\mathbf{Q}_w \triangleq [w^0\mathbf{I}_{N_r}, w^1\mathbf{I}_{N_r}, ..., w^D\mathbf{I}_{N_r}]^T \in \mathbb{R}^{N_r(D+1)\times N_r}$. In (9) $\beta_w \in \mathbb{R}$ stands for a weighting coefficient given by $\beta_w = \lambda^{t-w}$ where $\lambda \in \mathbb{R}$ is referred to as a forgetting factor. The exponential weighted RLS algorithm is implemented as follows:

$$\begin{aligned} \boldsymbol{\zeta}_t &= \boldsymbol{\Phi}_{t-1}^{-1}\mathbf{Q}_t x_t \in \mathbb{C}^{N_r(D+1)\times 1}, \\ \alpha_t &= \frac{1}{\lambda + \boldsymbol{\zeta}_t^\dagger \mathbf{Q}_t x_t} \in \mathbb{R}, \\ \boldsymbol{\Phi}_t^{-1} &= \lambda^{-1}\boldsymbol{\Phi}_{t-1}^{-1} - \lambda^{-1}\alpha_t \boldsymbol{\zeta}_t\boldsymbol{\zeta}_t^\dagger \in \mathbb{C}^{N_r(D+1)\times N_r(D+1)}, \\ e_t &= y_t - \widehat{\mathbf{H}}x_t \in \mathbb{C} \\ \widehat{\mathbf{H}}_{t+1} &= \widehat{\mathbf{H}}_t + \alpha_t e_t \zeta_t^\dagger \in \mathbb{C}^{1\times N_r(D+1)}. \end{aligned}$$

For initialization, $\widehat{\mathbf{H}}_1$ is considered to be identically zero and $\boldsymbol{\Phi}_0^{-1}$ is set to $\varrho\mathbf{I}_{N_r(D+1)}$ where $\varrho \gg 1$ is a constant with sufficiently large value. Moreover, x_1 is assumed to be a pilot symbol. The channel estimate $\widehat{\mathbf{H}}_{t+1}$ is then used to detect the $(t+1)^{th}$ symbol x_{t+1}.

2) NDA w. pilot ML estimator: We consider the expectation maximization (EM) based ML estimator developed in [8]. The new estimator uses pilot and data symbols jointly in order to track the channel variations. The pilot mapping used for the "NDA with pilot" ML estimator is described in Fig. 1. In a first step and for a given sub-carrier, the NDA with pilot estimator relies on pilot symbols to estimate the channel coefficients at pilot OFDM symbols as described in Section II-A2. In a second step, the NDA with pilot estimator applies the EM algorithm over all the received samples in order to jointly estimate the channel coefficients and detect the transmitted unknown symbols at non-pilot positions as well. The iterative EM algorithm runs in two main steps and uses as initialization $\widehat{\mathbf{c}}_{k,\mathrm{DA}}$ obtained in (8) from pilot positions only.

• Expectation step (E-Step):

During the E-Step, the pdf function defined in (6) takes into account all the possible transmitted symbols $\{a_m\}_{m=1}^{M}$ where M is the modulation order. In fact, at each iteration q, for every approximation window of size N_{NDA} symbols, the objective function is updated as follows:

$$Q(\mathbf{c}_k \mid \widehat{\mathbf{c}}_k^{(q-1)}) = -N_{\mathrm{NDA}} N_r \ln(2\pi\sigma^2) - \frac{1}{2\sigma^2}\sum_{r=1}^{N_r}\left(M_{2,k}^{(r)} + \sum_{n=1}^{N_{\mathrm{NDA}}} \alpha_{n,k}^{(q-1)} |\mathbf{c}_{r,k}^T \mathbf{t}(n)|^2 - 2\beta_{r,n,k}^{(q-1)} \mathbf{c}_{r,k}\right), \quad (10)$$

where $M_{2,k}^{(r)} = E\{|y_{r,k}(n)|^2\}$ is the second-order moment of the received samples over the r^{th} receiving antenna branch, $\mathbf{t}(n) = [1, t_n, t_n^2, ..., t_n^{J-1}]^T$ and:

$$\alpha_{n,k}^{(q-1)} = \sum_{m=1}^{M} P_{m,n,k}^{(q-1)} |a_m|^2, \quad (11)$$

$$\beta_{r,n,k}^{(q-1)}(\mathbf{c}_{r,k}) = \sum_{m=1}^{M} P_{m,n,k}^{(q-1)} \Re\{y_{r,k}^*(n) a_m \mathbf{t}^T(n) \mathbf{c}_{i,k}\}. \quad (12)$$

Here, $P_{m,n,k}^{(q-1)} = P(a_m \mid \mathbf{y}_k(n); \widehat{\mathbf{c}}^{(q-1)})$ is the *a posteriori* probability of a_m at iteration $(q-1)$ that is computed using the Bayes' formula as follows:

$$P_{m,n,k}^{(q-1)} = \frac{P(a_m) P\left(\mathbf{y}_k(n) | a_m; \widehat{\mathbf{c}}_k^{(q-1)}\right)}{P\left(\mathbf{y}_k(n); \widehat{\mathbf{c}}_k^{(q-1)}\right)}. \quad (13)$$

Since the symbols are assumed to be equally likely transmitted, we have $P(a_m) = \frac{1}{M}$ and therefore:

$$P\left(\mathbf{y}_k(n); \widehat{\mathbf{c}}_k^{(q-1)}\right) = \frac{1}{M}\sum_{m=1}^{M} P\left(\mathbf{y}_k(n) | a_m; \widehat{\mathbf{c}}_k^{(q-1)}\right). \quad (14)$$

• Maximization step (M-Step):

During the M-Step, the objective function obtained in (10) is maximized with respect to $\mathbf{c}_k$:

$$\widehat{\mathbf{c}}_k^{(q)} = \underset{\mathbf{c}_k}{\operatorname{argmax}}\, Q(\mathbf{c}_k | \widehat{\mathbf{c}}_k^{(q-1)}), \quad (15)$$

yielding the following more refined estimates for the approximation polynomial coefficients, i.e.:

$$\widehat{\mathbf{c}}_{r,k}^{(q)} = \left(\sum_{n=1}^{N_{\mathrm{NDA}}} \mathbf{t}(n)\mathbf{t}^T(n)\right)^{-1} \sum_{n=1}^{N_{\mathrm{NDA}}} \lambda_{r,n,k}^{(q-1)} \mathbf{t}(n). \quad (16)$$

In (16), $\lambda_{r,n,k}^{(q-1)}$ is given by:

$$\lambda_{r,n,k}^{(q-1)} = \left[\widehat{a}_k^{(q-1)}(t_n)\right]^* y_{r,k}(t_n), \quad (17)$$

in which

$$\widehat{a}_k^{(q-1)}(t_n) = \sum_{m=1}^{M} P_{m,n,k}^{(q-1)} a_m, \quad (18)$$

is the soft symbol estimate at iteration $q-1$ and $\mathbf{t}(\mathrm{n}) = [1, t_n, t_n^2, ..., t_n^{J-1}]^T$.

C. NDA or blind mode

For blind or NDA channel estimation, no pilot symbols are exploited by the receiver. Channel estimation is performed based on the information carried by all symbols assumed unknown a priori. Phase ambiguity is resolved by differential modulation. The blind RLS channel estimator algorithm is already the one described in Section II-B1. However, an arbitrary guess of the first sent symbol is used to initialize the recursive algorithm. The blind channel estimation algorithm is also the one described in Section II-B2. The only difference here, however, is that the initialization is arbitrary and random.

D. Data detection modes

On the top of selecting the appropriate channel estimator and pilot-use couples among DA ML, NDA w. pilot ML, NDA ML, DA LS, NDA w. pilot RLS and NDA RLS, the new context-aware CTR selects one of the following data detection modes:
• Coherent if pilot symbols are used.
• Non coherent or differential if no pilot symbols are used.
We also implement a "fully differential" transceiver version for which no channel estimation is required. Data detection is only based on differential modulation-demodulation. We use the soft-decision-aided DAPSK detection algorithm developed in [12] and [13].

III. Simulation setup and results

A 1×2 antenna configuration (1 transmit antenna at the eNodeB and 2 receive antennas at the mobile) is adopted as a SIMO configuration example for discussion in the rest of this paper. In the following, exhaustive computer simulations will be conducted in order to assess the performance of the newly proposed CTR transceivers at both the link- and system-levels.

A. Link-level simulations

In this subsection, link-level simulations assuming only one base station and a single mobile user are used to draw decision rules regarding:

1) The best channel identification mode [among DA, NDA w. pilot (i.e., hybrid), and completely NDA] that yields the highest link-level throughput.
2) The best detection scheme between coherent and differential detection depending on whether pilot symbols can be properly exploited or not at the receiver, respectively.
3) The best modulation-coding CQI couple among the conventional coherent (CQI-C) and the newly-designed differential (CQI-D) ones (cf. Tab. III discussed below).

The decision rules are drawn out against the operating conditions in terms of SNR, channel model type, mobile speed, and CQI value. Most significant LTE DL link-level parameters are summurized in Tab. I.
We consider a Pedestrian A (PedA) flat-fading channel model for users with mobile speed of 2 km/h and Vehicular A (VehA) and B (VehB) frequency-selective channels for users with mobile speeds of 30 km/h and 100 km/h. Their power delay profiles (PDPs) are given in Tab. II.
In order to account for adaptive modulation and coding (AMC), a CQI value indicates to the eNodeB the modulation order

TABLE I. LINK-LEVEL SIMULATIONS PARAMETERS.

Number of User Equipments	1
Channel bandwidth (MHz)	1.4
Carrrier frequency (GHz)	2.1
Frame duration (ms)	10
Subframe duration (ms)	1
Sub-carrier spacing (KHz)	15
FFT size	128
Number of resource blocks	6
Number of subcarriers/RB	12
DL bandwidth efficiency	77.1%
OFDM symbols subframe	7
CP length (μs)	5.2 (first symbols) 4.69 (six following symbols)
Transmit mode	SIMO
Channel types	PedA, VehA, and VehB
Channel coding	Convolutional turbo encoder

TABLE II. MULTIPATH POWER DELAY PROFILE.

Channel type	Relative Delay (ns)	Relative power (dB)
PedA	0	0
	110	-9.7
	190	-19.2
	410	-22.8
VehA	0	0
	310	-1
	710	-9
	1090	-10
	1730	-15
	2510	-20
VehB	0	-2.5
	300	0
	8900	-12.8
	12900	-10
	17100	-25.2
	20000	-16

and the channel coding rate adopted in each subframe. As highlighted in Table III, the CQI value ranges between 1 and 15 defining, respectively, six, three, and six possible coding rates for QPSK/DQPSK, 16QAM/D16Star-QAM, and 64QAM/D64Star-QAM modulations. Note that CQI-C and CQI-D stand for coherent and differential detection modulations, respectively. In our simulations, the CQI values as well as the SNR are assumed to be perfectly known at the receiver side. Assessment of CQI feedback and delay errors are beyond the scope of this contribution.

TABLE III. AMC SCHEMES USED BY LTE DL SIMULATOR.

CQI-C\CQI-D	Modulation	Coding rate
1	QPSK\DQPSK	0.0762
2	QPSK\DQPSK	0.1172
3	QPSK\DQPSK	0.1885
4	QPSK\DQPSK	0.3008
5	QPSK\DQPSK	0.4385
6	QPSK\DQPSK	0.5879
7	16QAM\D16StarQAM	0.3691
8	16QAM\D16StarQAM	0.4785
9	16QAM\D16StarQAM	0.6016
10	64QAM\D64StarQAM	0.4551
11	64QAM\D64StarQAM	0.5537
12	64QAM\D64StarQAM	0.6504
13	64QAM\D64StarQAM	0.7539
14	64QAM\D64StarQAM	0.8525
15	64QAM\D64StarQAM	0.9258

First, Fig. 2 shows the decision rules for the first proposed CTR (denoted hereafter as "CTR LS") that switches between the fully differential mode an the different LS channel estimation schemes: namely DA LS, NDA w. pilot LS, and NDA LS. The associated link-level throughput gains are also depicted in the same figure. The CTR LS can achieve up to 70% of link-level throughput gains over the traditional DA LS that operates with no cognition at all. Fig. 3 also shows that cognition can bring huge performance gains to the ML-based transceiver recently proposed in [8]. In fact, Fig. 3 depicts the identified decision rules and the associated link-level throughput gains (against

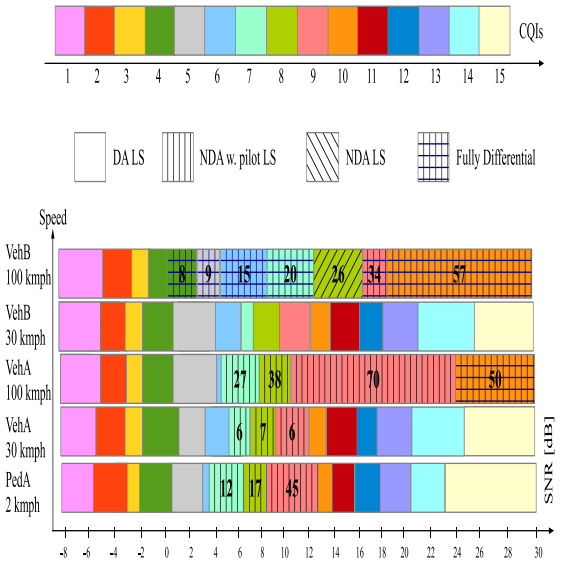

Fig. 2. Decision rules of the cognitive LS transceiver (CTR LS) and throughput gain percentages against the conventional DA LS estimator with coherent detection versus SNR for different channel types and mobile speeds.

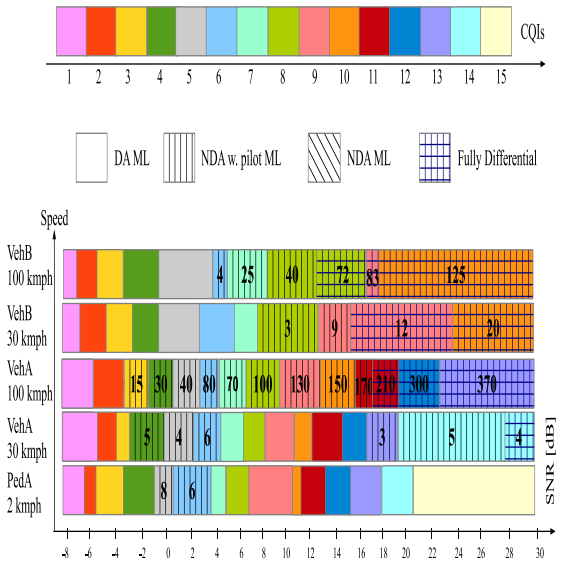

Fig. 3. Decision rules of the cognitive ML transceiver (CTR ML) and throughput gain percentages against the DA ML estimator with coherent detection versus SNR for different channel types and mobile speeds.

DA ML) for the second proposed CTR (denoted hereafter as "CTR ML") that switches between the fully differential detection mode and the different ML channel estimation schemes: namely DA ML, NDA w. pilot ML, and NDA ML. The associated link-level throughput gains are also depicted in the same figure and they can be as high as 370%. They can even reach 700% when compared to the conventional DA LS transceiver with no cognition as seen in Fig. 4.

In Fig. 5, we also compare the two newly proposed cognitive transceivers (i.e., CTR LS and CTR ML). It is seen that cognition is more advantageous when applied to our new ML estimator. In fact, CTR ML can offer a throughput gain as high as 600% over CTR LS.

Fig. 6, however, depicts the link-level throughput gains for a third but smarter cognitive transceiver denoted hereafter simply as

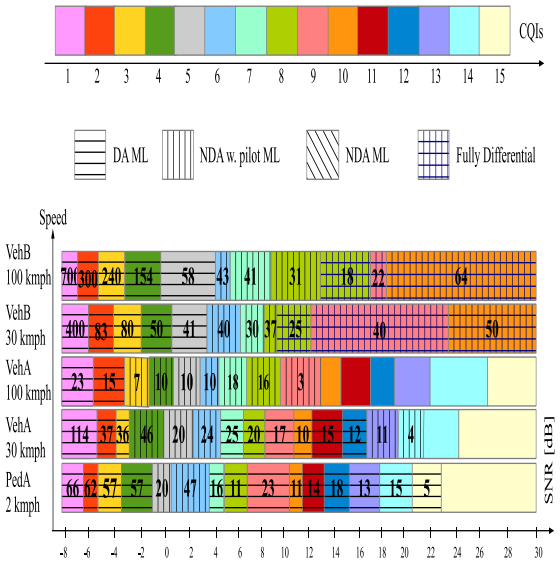

Fig. 4. Decision rules of the cognitive ML transceiver (CTR ML) and throughput gain percentages against the conventional DA LS estimator with coherent detection versus SNR for different channel types and mobile speeds.

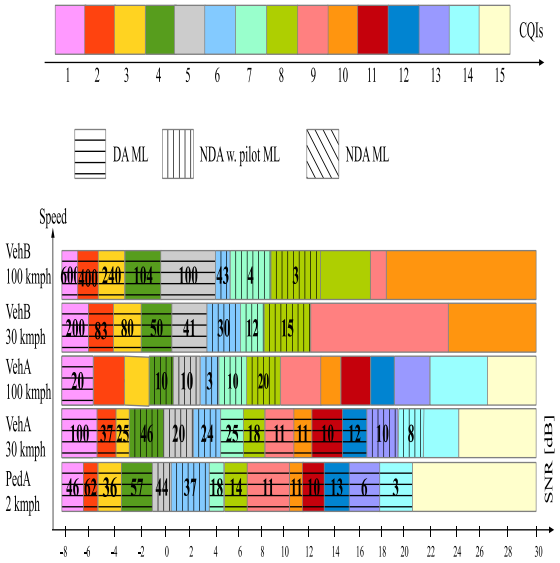

Fig. 5. Decision rules of the cognitive ML transceiver (CTR ML) and throughput gain percentages against the cognitive LS transceiver (CTR LS) versus SNR for different channel types and mobile speeds.

"CTR". In fact, CTR is able to switch between all the detection modes and channel estimation schemes listed previously for both CTR ML and CTR LS. By comparing Fig. 6 to Figs. 4 and 2 where DA LS is a common benchmark in all figures, it becomes clear that CTR exhibits indeed the highest throughput gains over CTR ML and CTR LS for every and each quadruplet (channel type, CQI value, SNR level, mobility speed).

B. System-level simulations

The link-level-based decision rules, identified in the previous subsection, are then assigned to a HetNet LTE DL system-level simulator in order to assess the performance of the new cognitive transceivers under more realistic conditions that take into account the interference effects of all network elements. More specifically,

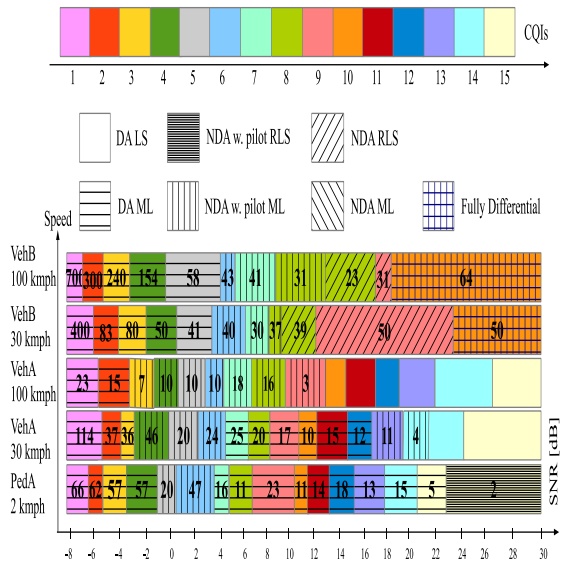

Fig. 6. Decision rules of the cognitive transceiver, CTR, and the throughput gain percentages against the conventional DA LS receiver (with coherent detection) versus SNR for different channel types and mobile speeds.

we simulate a 7-hexagonal-cell network with pico-cells dropped randomly in each macro area. An exhaustive list of the system-level parameters we used during our simulations is provided in Tab.IV. We also assume that 50% of the users move with a speed

TABLE IV. SYSTEM-LEVEL SIMULATION PARAMETERS.

Macrocell parameters	
Cellular layout	Hexagonal grid, 7 cell sites with BTS in the center of the cell
Inter-site distance	500 meters
Minimum UE to macro-BS distance	35 meters
Path loss model	TS 36.942, subclause 4.5.2
Antenna pattern	3-dimensional TS 36.942
TX antennas	1
Shadowing	Log-normal with 10 dB standard deviation
LTE BS antenna gain after cable loss	15 dBi
Macro BS antenna height	32 meters
Maximum macro-BS TX power	43 dBm
MCL	70 dBm
Scheduling algorithm	Round Robin
Resource Block width	180 kHz, total 12 RBs per subframe
Pico-cell parameters	
Cellular layout	Circular shape with BTS in the center of cell
Minimum distance between pico pNodeBs	40 meters
Minimum distance between new node and regular nodes	75 meters
Minimum UE to pico-BS distance	10 meters
Path loss model	TS 36.942, subclause 4.5.2
Antenna pattern	Omnidirectional
TX antennas	1
shadowing	Log-normal with 10 dB standard deviation
Antenna gain	5 dBi
Maximum pico-DS TX power	30 dBm
Scheduling algorithm	Round Robin
UE parameters	
UE distribution	High clustering: 2/3 of UEs dropped in the hotspots; others dropped uniformly over the macro-cell area (including hotspots)
UE Rx antennas	2
UE antenna gain	0 dBi
UE noise figure	9 dB
Number of UEs per cell-site area	60

of 2 kmph and experiencing PedA channel type. Moreover, 30%

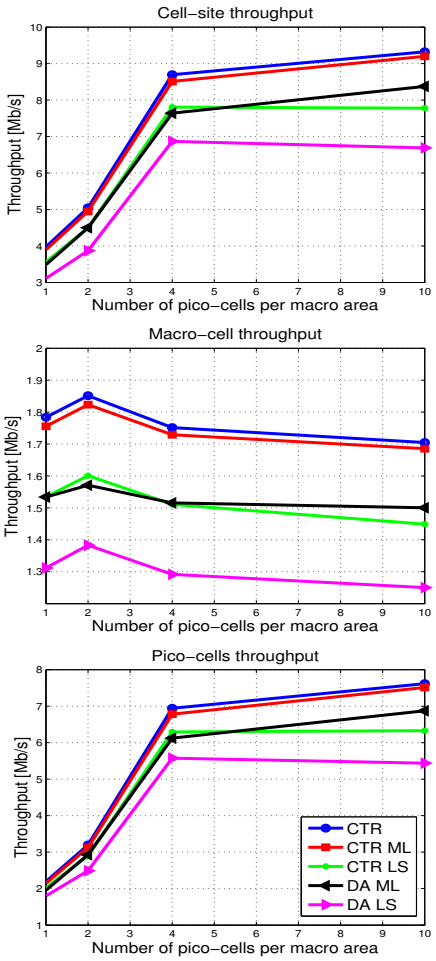

Fig. 7. System-level downlink throughput for the cell-site, macro-cell and pico-cells.

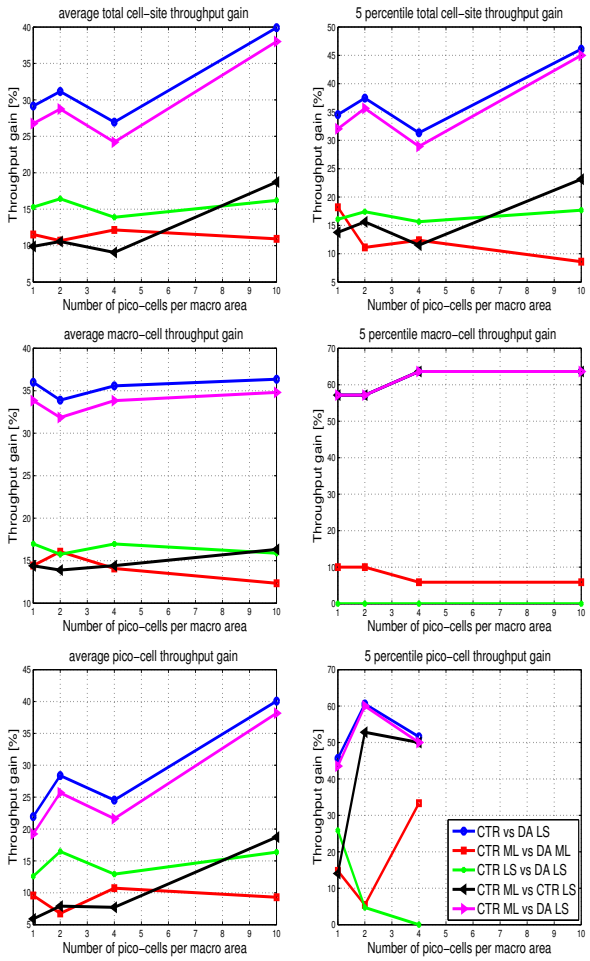

Fig. 8. System-level throughput gains

and 20% of the users are assumed to have a speed of 30 and 100 kmph, respectively. Medium and high speed users experience a VehA channel type and we simulate $\{1, 2, 4, 10\}$ pico-cells in each macro area as defined in [15]. This corresponds to $\{40, 20, 10, 4\}$ UEs in each pico area (cf. Tab. IV). Hereafter, we show the simulation results for the whole cell site, the central macro-cell as well as its pico-cells.

Fig. 9 shows system-level LTE DL throughput CDFs for DA ML, DA LS, CTR ML, CTR LS, and CTR transceivers. In all considered cases, CTR always delivers the highest throughput with overwhelming probability among all transceivers. Fig. 7 shows the impact of the number of dropped pico cells per-macro area on the different cognitive transceivers. The average DL system-level throughput increases with the number of picocells with maximum values achieved by the ML-based CTRs.

Fig.8, however, shows the "average" and "5^{th} percentile" (cell-edge) DL throughput gains at the system level. Huge performance gains are achieved by combining the cognitive transceiver concept and the new channel estimator recently introduced in [8]. In fact, in terms of cell-site performance, CTR ML and CTR exhibit about 40% and 45% of "average" and "5^{th} percentile" DL throughput gains, respectively. In terms of macro-cell performance, the "5^{th} percentile" (i.e., cell-edge) gains can even reach 60%. Note here that the 5^{th} percentile gain is not defined in Fig.8 for pico-cells in case of "10 pico-cells dropped in the macro area" because the CDF starts from a value higher than 5% as shown in Fig. 9.d.2).

IV. Conclusion

In this paper, we developed a new SIMO context-aware CTR that is able to switch to the best performing modem in terms of link-level throughput. On the top of conventional adaptive modulation and coding (AMC), we allow the context-aware CTR to make best selection among three different pilot-utilization modes: conventional dDA) or pilot-assisted, non-DA (NDA) or blind, and NDA with pilot which is a newly proposed hybrid version between the DA and NDA modes. We also enable the CTR to make best selection between two different channel identification schemes: conventional least-square (LS) and newly developed maximum-likelihood (ML) estimators. Depending on whether pilot symbols can be properly exploited or not at the receiver, we further enable the CTR to make best selection among two data detection modes: coherent or differential. Owing to extensive and exhaustive simulations on the downlink (DL) of a long-term evolution (LTE) heterogeneous network (HetNet), we are able draw out the decision rules of the new CTR that identify the best combination triplet of pilot-use, channel-identification, and data-detection modes to achieve the best link-level throughput at any operating condition in terms of channel type, mobile speed, signal-to-noise ratio (SNR), and channel quality indicator (CQI). Realistic extensive simulations at the system level suggest that the new context-aware CTR outperforms the conventional transceiver (i.e., pilot-assisted LS-type channel estimation with coherent detection) by as much as 40 and 45% gains in average and cell-edge (i.e., 5-percentile) total throughput per macro-area with 10 pico-cells, respectively.

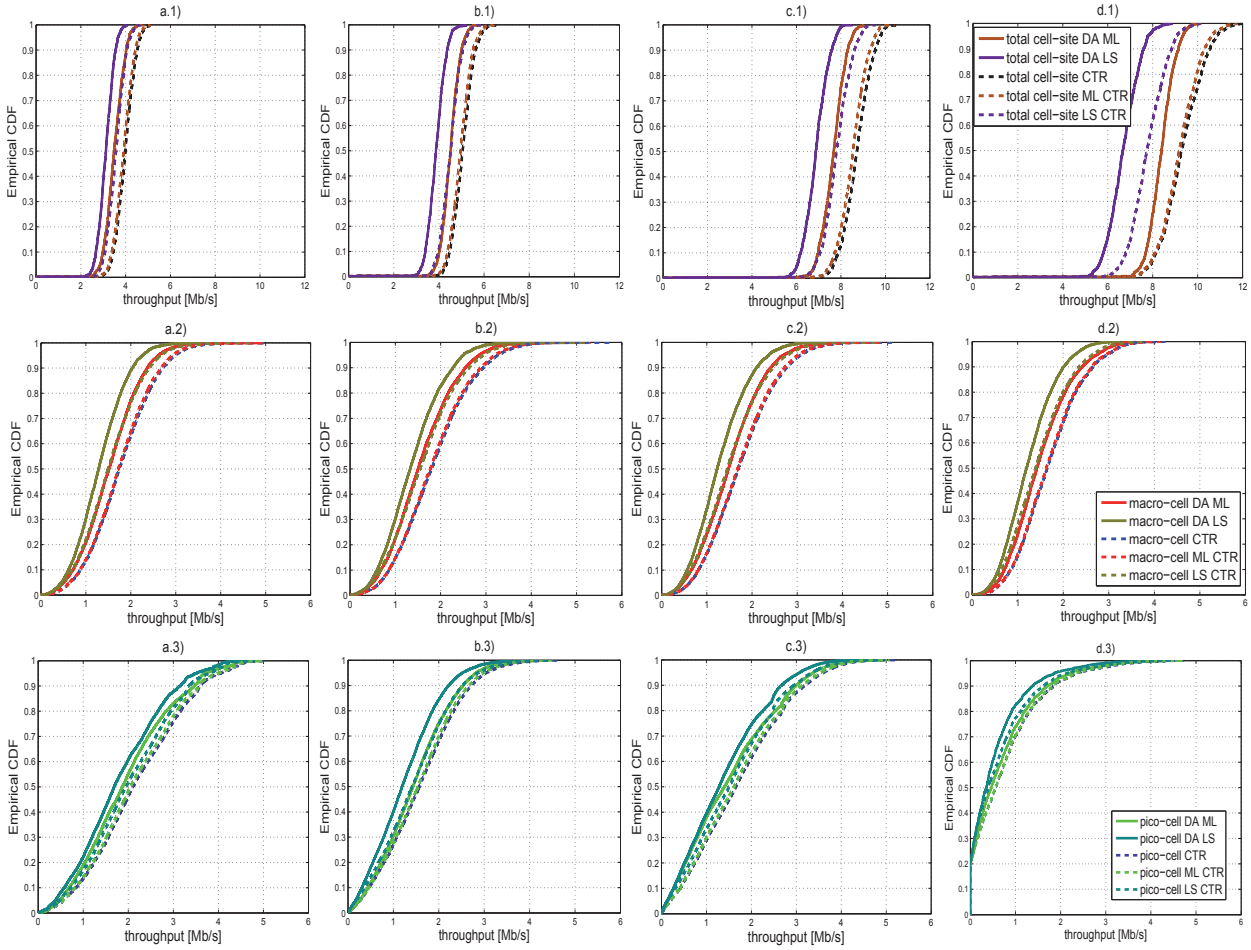

Fig. 9. HetNet LTE downlink System-level throughput performance for a) 1 pico-cell per macro area, b) 2 pico-cells per macro area, c) 4 pico-cells per macro area, and d) 10 pico-cells per macro area; 1) total cell-site, 2) macro-cell and 3) pico-cell.

REFERENCES

[1] F. Khan, *LTE-Advanced for 4G Mobile Broadband Air Interface Technologies and Performance*, Cambridge University Press, 2009.

[2] J. Mitola III, *Cognitive Radio Architecture*, John Wiley & Sons, 2006.

[3] S. Haykin, "Cognitive radio: brain-empowered wireless communications", *IEEE JSAC*, vol. 3, no. 2, pp. 201-220, Feb. 2005.

[4] W. Krenik, A.M. Wyglinski, and L.E. Doyle, "Cognitive radios for dynamic spectrum access", *IEEE TCOM*, vol. 45, no. 5, pp. 64-65, May 2007.

[5] J.W. Huang and V. Krishnamurthy, "Cognitive base stations in LTE/3GPP femtocells: a correlated equilibrium game-theoretic approach," *IEEE TCOM*, vol. 59, no. 12, pp. 3485-3493, Dec. 2011.

[6] A. Attar, V. Krishnamurthy, and O.N. Gharehshiran, "Interference management using cognitive base-stations for UMTS LTE," *IEEE Commun. Mag*, vol. 49, no. 8, pp. 152-159, Aug. 2011.

[7] J.-J. Van de Beek *et al* "On channel estimation in OFDM systems," in *Proc. IEEE 45th VTC*, 1995, vol. 2, pp. 815-819.

[8] F. Bellili, R. Meftehi, S. Affes, and A. Stéphenne, "Maximum likelihood SNR estimation of linearly-modulated signals over time-varying flat-fading SIMO channels," *IEEE TSP.*, vol. 63, no. 2, pp. 441-456. Jan. 2015.

[9] P. Bello, "Characterization of randomly time-variant linear channels," *IEEE TCOM*, vol. 11, no. 4, pp. 360-393, Dec. 1963.

[10] S. Omar , A. Ancora, and D.T.M. Slock, "Performance analysis of general pilot-aided linear channel estimation in LTE OFDMA systems with application to simplified MMSE schemes," in *Proc IEEE 19th PIMRC*, 2008.

[11] T.K. Akino, "Optimum weighted RLS channel estimation for rapid fading mimo channels," *IEEE TWireless*, vol. 7, no. 11, pp. 4248-4260, Nov. 2008.

[12] D. D. Liang, S. X. Ng. Soon, and L. Hanzo, "Soft-decision star-QAM aided BICM-ID," *IEEE SPL*, vol. 18, no. 3, pp. 169-172, Mar. 2011.

[13] C. Xu, D. Liang, S. X. Ng, and L. Hanzo, "Reduced-complexity noncoherent soft-decision-aided DAPSK dispensing with channel estimation," *IEEE TVT*, vol. 62, no. 6, pp. 2633- 2643, July 2013.

[14] 3GPP Standard TS 36.211 V8.2.0 (2008-03).

[15] 3GPP TR 36.814 V9.0.0 (2010-03).